

Universal Non-Hermitian Transport in Disordered Systems

Bo Li^{1,2} Chuan Chen^{1,2} and Zhong Wang^{1,2,*}

¹*MOE Key Laboratory for Nonequilibrium Synthesis and Modulation of Condensed Matter,
Shaanxi Province Key Laboratory of Quantum Information and Quantum Optoelectronic Devices,
School of Physics, Xi'an Jiaotong University, Xi'an 710049, China*

²*Institute for Advanced Study, Tsinghua University, Beijing 100084, China
³Lanzhou Center for Theoretical Physics, Key Laboratory of Quantum Theory and Applications of MoE,
Key Laboratory of Theoretical Physics of Gansu Province, and School of Physical Science and Technology,
Lanzhou University, Lanzhou, Gansu 730000, China*



(Received 11 January 2025; accepted 6 June 2025; published 15 July 2025)

In disordered Hermitian systems, localization of energy eigenstates prohibits wave propagation. In non-Hermitian systems, however, wave propagation is possible even when the eigenstates of a Hamiltonian are exponentially localized by disorders. We find in this regime that non-Hermitian wave propagation exhibits novel universal scaling behaviors without Hermitian counterpart. Furthermore, our theory demonstrates how the tail of imaginary-part density of states dictates wave propagation in the long-time limit. Specifically, for the three typical classes, namely the Gaussian, the uniform, and the linear imaginary-part density of states, we obtain logarithmically suppressed sub-ballistic transport, and two types of subdiffusion with exponents that depend only on spatial dimensions, respectively. Our work highlights the fundamental differences between Hermitian and non-Hermitian Anderson localization, and uncovers unique universality in non-Hermitian wave propagation.

DOI: 10.1103/z9m1-3mwb

The Anderson localization is one of the most prominent phenomena in random systems [1]. In recent years, the rapid development of non-Hermitian physics has sparked growing interest in the interplay between non-Hermiticity and Anderson localization. This has led to the discovery of many intriguing phenomena unique to non-Hermitian systems, including non-Hermitian Anderson transition [2–16], topological Anderson insulator [17–20], many-body localization [21–25], Lifshitz tail states [26–28], universality of non-Hermitian random matrices [29,30], erratic non-Hermitian skin localization [31], and anomalous dynamics [32–40].

The Anderson localization has twofold meanings. The spectral meaning is the localization of eigenstates, while the dynamic meaning is the absence of diffusion. It is generally perceived that the spectral localization always implies dynamical localization. For example, when the electron eigenstates at the Fermi level are Anderson localized, electron transport is prohibited in a crystal, resulting in insulating behavior at low temperature. In sharp contrast to this scenario, recent experiments in open or non-Hermitian systems have found that, despite complete localization of eigenstates, wave propagation remains possible [33,34] (see also related works Refs. [35–40]). In these systems, random gain and loss localize all the

eigenstates, yet waves can propagate in a jumpy manner, dynamically evading the localization.

Experimental and numerical findings suggest that this unconventional non-Hermitian transport dramatically differs from typical ballistic or diffusive motions in terms of the relationship between spreading distance and timescale [33]. It is also recognized that the complexity of eigen energies is essential, indicating the intrinsically non-Hermitian nature of the phenomenon. However, it remains elusive whether the observed unusual dynamics obeys universal laws. Here, we present a quantitative theory that yields universal transport dynamics, which not only explains the previous experimental findings but also predicts new scaling behaviors. The universality in this context manifests in the following aspects: (i) the space-time scaling of wave spreading is governed by the imaginary-part density of states, particularly its tail behavior; (ii) the scaling behavior depends solely on the dimensionality and the nature of the disorder, independent of other system-specific details; (iii) for weak disorders, the scaling approaches a universal form. Our theory highlights the fundamental differences between Hermitian and non-Hermitian Anderson localization, and provides an efficient scheme for calculating the universal behaviors from the basic data of the system. Our approach bears some similarity to Mott's variable-range hopping, though the mechanism is quite different [41]. Roughly speaking, the time plays the role of inverse temperature in Mott's picture.

*Contact author: wangzhongemail@tsinghua.edu.cn

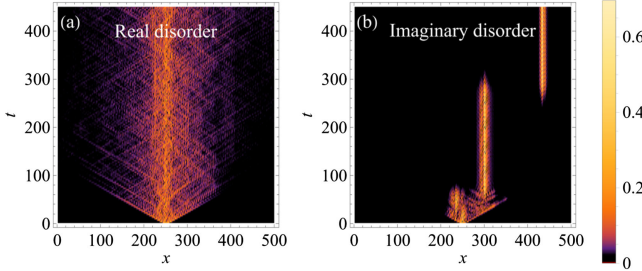


FIG. 1. The space-time evolution of a wave packet initially localized at the center of a chain is plotted under (a) real and (b) imaginary disorder, as described by Eq. (1) (For the real disorder scenario, the imaginary unit in front of the potential is omitted). Here, the disorder follows a uniform distribution $V_x \in [-W, W]$, and $t_0 = 2W = 1$ is used in the plots.

Dynamical scaling from an optimization—To be concrete, we consider a particle moving in a purely imaginary disorder potential,

$$H = \sum_{\langle \mathbf{x}, \mathbf{x}' \rangle} t_0 (|\mathbf{x}\rangle\langle \mathbf{x}'| + \text{H.c.}) + i \sum_{\mathbf{x}} V_{\mathbf{x}} |\mathbf{x}\rangle\langle \mathbf{x}|, \quad (1)$$

where $\langle \mathbf{x}, \mathbf{x}' \rangle$ stands for the nearest sites on a square-lattice model, t_0 is real, and $V_{\mathbf{x}}$ is a real site-dependent random variable. This model naturally arises in various contexts; for example, it describes classical wave propagation in a lattice with random gain and loss [33] and the dynamics of quantum particles in stochastic dissipative environments (see below). Note that our main results remain applicable if the random potential takes generic complex values, though we shall focus on the simplest cases with purely imaginary values. Numerical simulation of wave spreading exhibits a jumpy behavior [Fig. 1(b)], which is prominently different from the real-valued-disorder case with wave confined in a localization length [Fig. 1(a)].

Similar to the standard Anderson model, the eigenstates of this Hamiltonian exhibit exponential localization [33,42]. However, the eigenvalues now take random complex values. We label the eigenvalues $E_{\mathbf{x}} (\in \mathbb{C})$ and eigenstates $|\psi_{\mathbf{x}}\rangle$ by the localization center \mathbf{x} . Suppose that a particle or wave packet is initially located at $\mathbf{x} = \mathbf{0}$. Its time evolution can be conveniently analyzed in the eigenbasis, i.e., $|\phi(t)\rangle = \sum_{\mathbf{x}} a_{\mathbf{x}}(t) |\psi_{\mathbf{x}}\rangle$, where the coefficient has modulus $|a_{\mathbf{x}}(t)| \sim e^{-|\mathbf{x}|/\xi + \lambda_{\mathbf{x}} t}$, ξ being the eigenstate localization length and $\lambda_{\mathbf{x}} = \text{Im}(E_{\mathbf{x}})$. The wave intensity (or particle density) at a position \mathbf{x} at time t is $P(\mathbf{x}, t) \sim e^{2W(\mathbf{x}, t)}$, where $W(\mathbf{x}, t) = -|\mathbf{x}|/\xi + \lambda_{\mathbf{x}} t$ is a weight factor. At each moment, the wave-center spreading distance $|\mathbf{x}_c| = \sum_{\mathbf{x}} |\mathbf{x}| P(\mathbf{x}, t) / \sum_{\mathbf{x}} P(\mathbf{x}, t)$ is dominated by the localization center of the eigenstate with maximum weight factor, and contributions from other eigenstates are exponentially suppressed. The weight factor measures the competition between the exponential tail suppression ($-|\mathbf{x}|/\xi$) and the temporal amplification ($\lambda_{\mathbf{x}} t$). As time

grows, the most probable localization center moves to further positions, spreading the wave packet over space. Therefore, the average displacement is obtained by optimizing the weight factor at each moment [41,43–49].

To implement this optimization, we estimate the largest growing factor $\lambda_{|\mathbf{x}|}^{\max}$ within a volume $\sim |\mathbf{x}|^d$. Since $\lambda_{\mathbf{x}}$ follows the same distribution across each site, $W(\mathbf{x}, t)$ is predominantly optimized by $\lambda_{|\mathbf{x}|}^{\max}$ within this volume. This is particularly relevant given the broad distribution of $\lambda_{\mathbf{x}}$ under strong randomness, leading to an exponential suppression of other contributions. The probability of selecting a value greater than $\lambda_{|\mathbf{x}|}^{\max}$ is $P_{|\mathbf{x}|} = \int_{\lambda_{|\mathbf{x}|}^{\max}}^{\infty} d\lambda \rho(\lambda)$, where $\rho(\lambda)$ is the imaginary-part density of states (ImDOS). Specifically, $\rho(\lambda)$ is defined as $\rho(\lambda) = \int_{-\infty}^{\infty} d\epsilon \rho(\epsilon, \lambda)$, where $\rho(\epsilon, \lambda)$ represents the density of states for the complex energy $\epsilon + i\lambda$ in the complex plane. In the considered region, there has to be at least one site taking the value $\lambda_{|\mathbf{x}|}^{\max}$, implying $P_{|\mathbf{x}|} |\mathbf{x}|^d \sim 1$. This yields [50]

$$P_{|\mathbf{x}|} \sim |\mathbf{x}|^{-d}, \quad (2)$$

meaning that $P_{|\mathbf{x}|}$ should diminish as $|\mathbf{x}|$ grows. This indicates that the long-time scaling behavior is dictated by the tail of ImDOS. If ImDOS $\rho(\lambda)$ is specified, the relation between $\lambda_{|\mathbf{x}|}^{\max}$ and $|\mathbf{x}|$ can be further identified with the help of Eq. (2). For instance, if the ImDOS follows the Gaussian distribution $\rho(\lambda) \propto e^{-\lambda^2/(2\sigma^2)}$ with σ being the standard deviation, by using the expansion of the error function we can obtain $\lambda_{|\mathbf{x}|}^{\max} \sim (d \ln |\mathbf{x}|)^{1/2}$ [53]. Substituting this relation into the weight factor and letting

$$\frac{dW}{d|\mathbf{x}|} = -\frac{1}{\xi} + \frac{d\lambda_{|\mathbf{x}|}^{\max}}{d|\mathbf{x}|} t = 0, \quad (3)$$

we arrive at the space-time scaling of spreading distance [53]

$$|\mathbf{x}_c| \sim \frac{t}{(\ln t)^{1/2}}, \quad (4)$$

which implies a sub-ballistic motion. For other distributions, the resulting scaling behaviors are summarized in Table I. Note that the scaling is determined by an integral of ImDOS with $\lambda_{|\mathbf{x}|}^{\max}$ being the lower bound. As $\lambda_{|\mathbf{x}|}^{\max}$ increases

TABLE I. Dynamical scaling for different ImDOS. For the linear ImDOS, a, b are real parameters. The domain of λ is given to ensure the normalization, not specified here.

ImDOS	$\rho(\lambda)$	Dynamical scaling
Gaussian	$e^{-\lambda^2/(2\sigma^2)}$	$ \mathbf{x}_c \sim t / (\ln t)^{1/2}$
Uniform	Constant	$ \mathbf{x}_c \sim t^{1/(d+1)}$
Linear	$a - b\lambda$	$ \mathbf{x}_c \sim t^{2/(d+2)}$

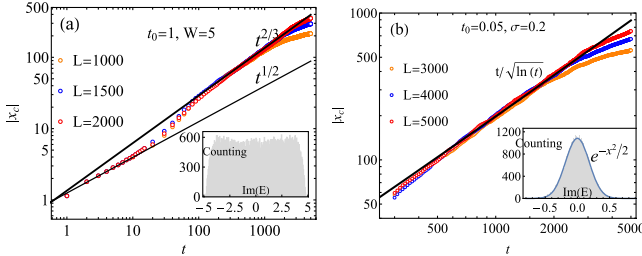


FIG. 2. Dynamical scaling in 1D lattice models with imaginary disorder. (a) For the uniform disorder, where $t_0 = 1$ and $W = 5$, simulations are conducted with 500 realizations of disorder. (b) Gaussian disorder with $t_0 = 0.05$ and $\sigma = 0.2$ is considered, with 1500 realizations of disorder. The data for $\text{Im}(E)$ in both insets are collected from a system with $L = 500$ and 200 trials of disorder.

with spatial distance and time, the effect of ImDOS will gradually fade away, leaving its small tail to become dominant in the late-stage dynamics. In this process, a crossover from one scaling to another may arise if the ImDOS does not take a universal functional form [e.g., the example in Fig. 2(a) discussed later].

To further clarify our approach, we compare it with Mott's variable-range hopping (VRH) [41]. In a strongly disordered system, electrons can hop between localized states a distance R apart with the aid of phonons. At low temperatures, the hopping probability is estimated as $P \sim e^{-2R/\xi - \Delta/(k_B T)}$, where ξ is the localization length and Δ is the energy difference between two states. The conductivity, governed by the most probable hopping process, results from an optimization between the spatial term $2R/\xi$, which favors short hops, and the energy term $\Delta/(k_B T)$, which benefits from larger hops to minimize energy differences. This optimization is achieved by approximating Δ as a function of R and solving $(\partial/\partial R)[2R/\xi + \Delta(R)/(k_B T)] = 0$ [54]. Notably, despite the entirely different physical pictures, the optimization process in our approach exhibits similarities to VRH, where $1/(k_B T)$ in VRH plays a role analogous to t in our dynamical scaling analysis.

1D examples with strong disorder—To validate our dynamic scaling predictions, we conducted numerical simulations for 1D cases. The spreading distance $|x_c| = \sum_x |x| |\langle x|\phi(t)\rangle|^2 / \langle \phi(t)|\phi(t)\rangle$ is numerically calculated and then averaged over various disorder configurations. In our initial exploration, we examined a uniform disorder potential with $V_x \in [-W, W]$. For sufficiently strong disorder, $W \gg t_0$, dominating the imaginary part of spectrum, the ImDOS is approximately a uniform distribution [$\rho(\lambda) = \text{const.}$] except for the linearly decreasing tail [$\rho(\lambda) \sim a - b\lambda$] near the edge, as depicted in the inset of Fig. 2(a). As a result, a $|x_c| \sim t^{1/(d+1)}|_{d=1} = t^{1/2}$ scaling appears in the early stage because $P_{|x|}$ in Eq. (2) is mainly dictated by a uniform ImDOS. However, the late-stage

scaling switches to $|x_c| \sim t^{2/(d+2)}|_{d=1} = t^{2/3}$ as a consequence of the linear tail of ImDOS. This prediction aligns well with numerical simulations in Fig. 2(a), where size-effect-free scaling is evident from the overlap between the curves for different system sizes. The deviation from the thermodynamic-limit trajectory is observed to be delayed for larger systems compared to smaller ones. Here, the linear ImDOS tail can be understood by the rare events of neighboring sites occupied by potentials with similar values [53]. Moreover, our theory and simulations are fully consistent with the optical experiment [33]. Another significant case involves Gaussian-type ImDOS, generated by strong Gaussian imaginary disorder with $\sigma \gg t_0$. As shown in Fig. 2(b), the numerical data for the larger-size system overlay on top of the smaller one until size effect entering the dynamics. The theoretical prediction in Eq. (4) matches perfectly with the overlapped part at a large time, owing to that Eq. (4) is justified for large λ .

Numerical results for 2D—In Table I, the uniform or linear ImDOS result in a dimension-dependent scaling, providing a key feature for verifying our predictions. Similar to the 1D case, a strong uniform disorder in higher dimension is expected to give a ImDOS with a linear tail attached to a uniform bulk part. In Fig. 3(a), we performed simulations for the 2D case, where $|x_c| \sim t^{1/(d+1)}|_{d=2} = t^{1/3}$ is indeed observed in the early dynamical stage. However, constraints on simulation size prevent the observation of late-stage dynamics influenced by the linear ImDOS tail. To address dimension sensitivity stemming from a linear ImDOS, simulations are conducted under the influence of strong imaginary disorder adhering to a (right angled) triangular distribution; i.e., the probability density follows $f(V_x) = 2(1 - V_x/c)/c$ with $V_x \in [0, c]$ and $t_0 \ll c$. Notably, the predominant linear ImDOS profile facilitates rapid manifestation prior to the onset of size effects, thus leveraging the limited size in 2D simulations effectively. In Fig. 3(b), the expected scaling $|x_c| \sim t^{2/(d+2)}|_{d=2} = t^{1/2}$ is evident during the early stage, while long-term dynamics are influenced by both size effects and the ImDOS tail, which is not of interest here.

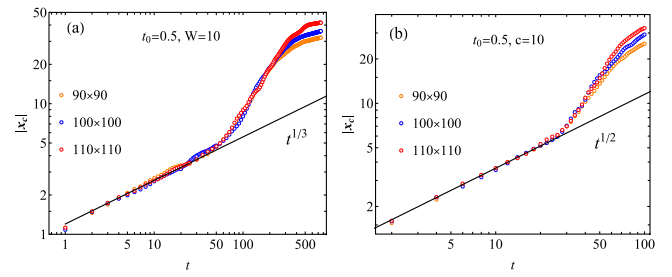


FIG. 3. Dynamical scaling for 2D square-lattice models with system size given by the plot legends, where 500 realizations of disorder are performed. (a) A uniform disorder $V_x \in [-W, W]$ is considered. (b) The disorder follows a right triangle distribution, where c is the length of the base line, see the text.

Universal scaling under weak disorder—In the preceding examples, we focused on the strong-disorder regime, where the imaginary part of the density of states (ImDOS) is predominantly shaped by the statistical properties of the disorder. As the disorder strength decreases, however, a universal Gaussian-type form of the ImDOS gradually emerges. In the weak-disorder limit, the localization length ξ spans many unit cells ($\xi \gg 1$), and within this length scale, particle spreading exhibits ballistic scaling, characterized by $|\mathbf{x}| \sim t$. Nonetheless, the earlier analysis remains applicable after coarse-graining and rescaling the length scale by ξ : the wave packet remains strongly localized in the rescaled system. Despite the coarse-grained unit cell is occupied by many eigenstates, the longtime ($t \gg 1$) probability of the wave packet locating at the new cell positioning at \mathbf{X} is mostly governed by the maximum growing factor $\lambda_{\mathbf{X}}$ therein, represented as $P(\mathbf{X}, t) \sim e^{-2|\mathbf{X}|/\xi+2\lambda_{\mathbf{X}}t}$, where $\lambda_{\mathbf{X}}$ follows the same distribution as the original $\lambda_{\mathbf{x}}$. Moreover, for sufficiently weak disorder, i.e., $\xi \gg 1$, the central limit theorem implies that $\lambda_{\mathbf{x}}$, which is approximated as an average of $V_{\mathbf{x}}$ within the volume of size ξ^d , follows a Gaussian distribution [53]. Consequently, the scaling behavior converges to the universal form given in Eq. (4) in the weak-disorder, thermodynamic limit. Nevertheless, its numerical validation necessitates exceptionally large system sizes, which will be left for future study.

The emerging Gaussian distribution is contingent upon condition $\xi \gg 1$, which gradually breaks down as disorder strength increases until the system approaches the regime of strong disorder, i.e., $\xi \lesssim 1$. In the case of intermediate disorder characterized by $W, \sigma \sim t_0$, the ImDOS cannot be sharply identified. Consequently, the associated scaling behavior undergoes an unknown crossover bridging the two extreme cases [53].

Renormalization group analysis—As explained above, the scaling behavior exhibits certain sensitivity to disorder strength. In the regime of weak disorders, our approach necessitates a rescaled interpretation. In this respect, it is helpful to view our problem from the renormalization group perspective. This not only validates our rescaled treatment for weak disorder cases but also suggests new scaling behaviors for the delocalized phase that is inaccessible to the previous approach. In long-wavelength limit, the Hamiltonian Eq. (1) is represented as a Schrödinger equation $i\partial_t\psi(\mathbf{x}, t) = [-D\nabla^2 + iV(\mathbf{x})]\psi(\mathbf{x}, t)$, where the potential obeys $\langle V(\mathbf{x})V(\mathbf{x}') \rangle = v\delta^d(\mathbf{x} - \mathbf{x}')$ with $v > 0$ representing the disorder strength. Performing the transformation $\psi(\mathbf{x}, t) = \exp(\Phi(\mathbf{x}, t))$, the Schrödinger equation is converted to a nonlinear equation,

$$\partial_t\Phi = iD\nabla^2\Phi + i\eta(\nabla\Phi)^2 + V(\mathbf{x}), \quad (5)$$

where $D = \eta = t_0$. This form allows us to implement a dynamical renormalization group analysis [55,56].

Following the standard procedure [57], we obtain a flow equation [53]

$$\frac{dg}{dl} = g \left[4 - d + \frac{2(12 - 5d)}{d} K_d g \right], \quad (6)$$

where $g = v\eta^2/D^4$, $K_d = S_d/(2\pi)^d$ with S_d being the solid angle in d dimension, and the rescaling $\mathbf{x} \rightarrow e^l\mathbf{x}$ is performed. The flow equation yields two fixed points, $g_1^* = 0$, $g_2^* = d(d-4)/[2(12-5d)K_d]$. Notably, g_1^* is unstable for $d < 4$, while g_2^* is physically untenable for $d < 12/5$ due to its negative value, conflicting with the definition. Thus, in 1D and 2D, the system does not transit to new phases upon rescaling, validating our analysis for weak disorders. However, for $d = 3$, $g_2^* = 1/(2K_d)$ is a genuine fixed point, signifying a delocalization transition. In the delocalized phase with weak disorder, the system's longtime behavior is governed by this fixed point, meaning the space-time relation remains invariant under rescaling. Consequently, the system exhibits dynamical scaling $|\mathbf{x}| \sim t^{3/5}$ [53]. This result is independent of the disorder statistics and beyond the approach outlined in Eqs. (2) and (3) which focuses on the eigenstate-localized regime.

Liouvillian dynamics—Although the preceding analysis focuses on systems with non-Hermitian Hamiltonians, it is noteworthy that analogous dynamics can arise within the framework of the Liouvillian superoperator. We consider an open system described by the following Lindblad master equation of density matrix $\hat{\rho}$:

$$\frac{d\hat{\rho}}{dt} = -i[\hat{H}_0, \hat{\rho}] + \sum_{\mathbf{x}} \gamma_{\mathbf{x}} \mathcal{D}[\hat{a}_{\mathbf{x}}] \hat{\rho}, \quad (7)$$

where $\hat{H}_0 = \sum_{\mathbf{x}, \mathbf{x}'} h_{\mathbf{x}, \mathbf{x}'} \hat{a}_{\mathbf{x}}^\dagger \hat{a}_{\mathbf{x}'}$ is a Hermitian Hamiltonian, with $\hat{a}_{\mathbf{x}}^\dagger (\hat{a}_{\mathbf{x}})$ being the creation (annihilation) operator at lattice site \mathbf{x} , and $\mathcal{D}[\hat{a}_{\mathbf{x}}] \hat{\rho} = \hat{a}_{\mathbf{x}} \hat{\rho} \hat{a}_{\mathbf{x}}^\dagger - \frac{1}{2} (\hat{a}_{\mathbf{x}}^\dagger \hat{a}_{\mathbf{x}} \hat{\rho} + \hat{\rho} \hat{a}_{\mathbf{x}}^\dagger \hat{a}_{\mathbf{x}})$. On the right-hand side of Eq. (7), the first term describes a unitary evolution given by \hat{H}_0 , and the second term accounts local losses with site-dependent random rate $\gamma_{\mathbf{x}}$. Using Eq. (7), we can show that two-point correlation function $G_{\mathbf{x}_1, \mathbf{x}_2} = \text{Tr}[\hat{\rho} \hat{a}_{\mathbf{x}_1}^\dagger \hat{a}_{\mathbf{x}_2}]$ satisfies the following matrix equation [53]:

$$\frac{dG}{dt} = i(HG - GH^\dagger), \quad (8)$$

where $G = \sum_{\mathbf{x}, \mathbf{x}'} G_{\mathbf{x}, \mathbf{x}'} |\mathbf{x}\rangle \langle \mathbf{x}'|$, and $H = h^T + iV$ describes a Hermitian system h^T subject to a random imaginary disorder iV with $V_{\mathbf{x}, \mathbf{x}'} = \gamma_{\mathbf{x}} \delta_{\mathbf{x}, \mathbf{x}'}$. The equation is solved by $G(t) = e^{iHt} G(0) e^{-iH^\dagger t}$. Considering N bosonic particles (e.g., photons in a cavity) initially locate at $\mathbf{x} = \mathbf{0}$, i.e., $G_{\mathbf{x}, \mathbf{x}'}(0) = N \delta_{\mathbf{x}, \mathbf{x}'} \delta_{\mathbf{x}, \mathbf{0}}$, the correlation matrix at time t evolves to $G(t) = N |\phi(t)\rangle \langle \phi(t)|$, where $|\phi(t)\rangle = e^{iHt} |\mathbf{0}\rangle$ acts as a “quantum state” dictated by the “Hamiltonian” H .

The probability distribution of surviving particles is given by $P(\mathbf{x}, t) = G_{\mathbf{x}, \mathbf{x}}(t) / \sum_{\mathbf{x}} G_{\mathbf{x}, \mathbf{x}}(t) = |\langle \mathbf{x} | \phi(t) \rangle|^2 / \langle \phi(t) | \phi(t) \rangle$. This coincides exactly with the particle evolution before, indicating the same dynamical scaling behavior in such an open system. Furthermore, similar dynamic behaviors can emerge from purely dissipative systems ($\hat{H}_0 = 0$) by considering suitable dissipators involving adjacent sites [34,53].

Conclusion—In systems featuring complex disorders, the nonunitary time evolution facilitates a particle's jumpy motion even amid eigenstate localization, in sharp contrast to the conventional Anderson localization. Employing an intuitive optimization approach, we unveiled the universal dynamical scaling in this unconventional non-Hermitian transport, distinctly different from typical diffusive or ballistic transport. More interestingly, we find a close connection between the scaling behavior and the imaginary-part density of states (ImDOS), especially the long-time behavior is dictated by the tail of ImDOS. Our findings underscore the fundamental distinction between non-Hermitian and Hermitian localization, particularly in terms of dynamics. Numerous open questions persist, including the theoretical prediction and experimental observation of dynamic behaviors arising from different types of disorders, particularly in the regime with comparable kinetic and potential terms. It is also interesting to explore the combined dynamical consequence of Anderson localization and non-Hermitian skin effect [3,10,58–69]. Additionally, the interplay between interactions and non-Hermitian disorders poses an intriguing avenue for exploration. On the experimental front, photonic systems provide a promising platform, as demonstrated by relevant experiments [33]. Furthermore, open systems featuring local random losses, such as dissipative cavity arrays, offer additional opportunities to validate our theory.

Acknowledgments—This work is supported by National Key R&D Program of China (Grant No. 2023YFA1406702) and NSFC under Grant No. 12125405. B. L. is partially supported by NSFC under Grant No. 12404185. C. C. acknowledges support from the NSFC under Grant No. 12347107.

Data availability—The data that support the findings of this Letter are not publicly available. The data are available from the authors upon reasonable request.

-
- [1] P. W. Anderson, Absence of diffusion in certain random lattices, *Phys. Rev.* **109**, 1492 (1958).
 - [2] N. Hatano and D. R. Nelson, Localization transitions in non-Hermitian quantum mechanics, *Phys. Rev. Lett.* **77**, 570 (1996).
 - [3] H. Jiang, L.-J. Lang, C. Yang, S.-L. Zhu, and S. Chen, Interplay of non-Hermitian skin effects and Anderson localization in nonreciprocal quasiperiodic lattices, *Phys. Rev. B* **100**, 054301 (2019).
 - [4] S. Longhi, Topological phase transition in non-Hermitian quasicrystals, *Phys. Rev. Lett.* **122**, 237601 (2019).
 - [5] S. Longhi, Metal-insulator phase transition in a non-Hermitian Aubry-André-Harper model, *Phys. Rev. B* **100**, 125157 (2019).
 - [6] Y. Huang and B. I. Shklovskii, Anderson transition in three-dimensional systems with non-Hermitian disorder, *Phys. Rev. B* **101**, 014204 (2020).
 - [7] T. Liu, H. Guo, Y. Pu, and S. Longhi, Generalized Aubry-André self-duality and mobility edges in non-Hermitian quasiperiodic lattices, *Phys. Rev. B* **102**, 024205 (2020).
 - [8] Q.-B. Zeng and Y. Xu, Winding numbers and generalized mobility edges in non-Hermitian systems, *Phys. Rev. Res.* **2**, 033052 (2020).
 - [9] K. Kawabata and S. Ryu, Nonunitary scaling theory of non-Hermitian localization, *Phys. Rev. Lett.* **126**, 166801 (2021).
 - [10] S. Weidemann, M. Kremer, S. Longhi, and A. Szameit, Topological triple phase transition in non-Hermitian Floquet quasicrystals, *Nature (London)* **601**, 354 (2022).
 - [11] X. Luo, T. Ohtsuki, and R. Shindou, Transfer matrix study of the Anderson transition in non-Hermitian systems, *Phys. Rev. B* **104**, 104203 (2021).
 - [12] X. Luo, T. Ohtsuki, and R. Shindou, Universality classes of the Anderson transitions driven by non-Hermitian disorder, *Phys. Rev. Lett.* **126**, 090402 (2021).
 - [13] Y. Liu, Q. Zhou, and S. Chen, Localization transition, spectrum structure, and winding numbers for one-dimensional non-Hermitian quasicrystals, *Phys. Rev. B* **104**, 024201 (2021).
 - [14] X. Luo, Z. Xiao, K. Kawabata, T. Ohtsuki, and R. Shindou, Unifying the Anderson transitions in Hermitian and non-Hermitian systems, *Phys. Rev. Res.* **4**, L022035 (2022).
 - [15] Y. Liu, Z. Wang, C. Yang, J. Jie, and Y. Wang, Dissipation-induced extended-localized transition, *Phys. Rev. Lett.* **132**, 216301 (2024).
 - [16] W. Wang, X. Wang, and G. Ma, Anderson transition at complex energies in one-dimensional parity-time-symmetric disordered systems, *Phys. Rev. Lett.* **134**, 066301 (2025).
 - [17] D.-W. Zhang, L.-Z. Tang, L.-J. Lang, H. Yan, and S.-L. Zhu, Non-Hermitian topological Anderson insulators, *Sci. China Phys. Mech. Astron.* **63**, 267062 (2020).
 - [18] L.-Z. Tang, L.-F. Zhang, G.-Q. Zhang, and D.-W. Zhang, Topological Anderson insulators in two-dimensional non-Hermitian disordered systems, *Phys. Rev. A* **101**, 063612 (2020).
 - [19] H. Liu, J.-K. Zhou, B.-L. Wu, Z.-Q. Zhang, and H. Jiang, Real-space topological invariant and higher-order topological Anderson insulator in two-dimensional non-Hermitian systems, *Phys. Rev. B* **103**, 224203 (2021).
 - [20] Q. Lin, T. Li, L. Xiao, K. Wang, W. Yi, and P. Xue, Observation of non-Hermitian topological Anderson insulator in quantum dynamics, *Nat. Commun.* **13**, 3229 (2022).
 - [21] R. Hamazaki, K. Kawabata, and M. Ueda, Non-Hermitian many-body localization, *Phys. Rev. Lett.* **123**, 090603 (2019).
 - [22] L.-J. Zhai, S. Yin, and G.-Y. Huang, Many-body localization in a non-Hermitian quasiperiodic system, *Phys. Rev. B* **102**, 064206 (2020).

- [23] K. Suthar, Y.-C. Wang, Y.-P. Huang, H. H. Jen, and J.-S. You, Non-Hermitian many-body localization with open boundaries, *Phys. Rev. B* **106**, 064208 (2022).
- [24] Y.-C. Wang, K. Suthar, H. H. Jen, Y.-T. Hsu, and J.-S. You, Non-Hermitian skin effects on thermal and many-body localized phases, *Phys. Rev. B* **107**, L220205 (2023).
- [25] F. Roccati, F. Balducci, R. Shir, and A. Chenu, Diagnosing non-Hermitian many-body localization and quantum chaos via singular value decomposition, *Phys. Rev. B* **109**, L140201 (2024).
- [26] F. M. Marchetti and B. D. Simons, Optimal fluctuations and tail states of non-Hermitian operators, *J. Phys. A* **34**, 10805 (2001).
- [27] P. G. Silvestrov, Extended tail states in an imaginary random potential, *Phys. Rev. B* **64**, 075114 (2001).
- [28] S. Longhi, Lifshitz tail states in non-Hermitian disordered photonic lattices, *Opt. Lett.* **50**, 746 (2025).
- [29] R. Hamazaki, K. Kawabata, N. Kura, and M. Ueda, Universality classes of non-Hermitian random matrices, *Phys. Rev. Res.* **2**, 023286 (2020).
- [30] Z. Chen, K. Kawabata, A. Kulkarni, and S. Ryu, Field theory of non-Hermitian disordered systems, *Phys. Rev. B* **111**, 054203 (2025).
- [31] S. Longhi, Erratic non-Hermitian skin localization, *Phys. Rev. Lett.* **134**, 196302 (2025).
- [32] M. Balasubrahmanyam, S. Mondal, and S. Majumdar, Necklace-state-mediated anomalous enhancement of transport in Anderson-localized non-Hermitian hybrid systems, *Phys. Rev. Lett.* **124**, 123901 (2020).
- [33] S. Weidemann, M. Kremer, S. Longhi, and A. Szameit, Coexistence of dynamical delocalization and spectral localization through stochastic dissipation, *Nat. Photonics* **15**, 576 (2021).
- [34] S. Longhi, Anderson localization in dissipative lattices, *Ann. Phys. (Berlin)* **535**, 2200658 (2023).
- [35] I. I. Yusipov, T. V. Laptyeva, and M. V. Ivanchenko, Quantum jumps on Anderson attractors, *Phys. Rev. B* **97**, 020301 (R) (2018).
- [36] A. F. Tzortzakakis, K. G. Makris, A. Szameit, and E. N. Economou, Transport and spectral features in non-Hermitian open systems, *Phys. Rev. Res.* **3**, 013208 (2021).
- [37] A. Leventis, K. G. Makris, and E. N. Economou, Non-Hermitian jumps in disordered lattices, *Phys. Rev. B* **106**, 064205 (2022).
- [38] H. Sahoo, R. Vijay, and S. Majumdar, Anomalous transport regime in a non-Hermitian Anderson-localized hybrid system, *Phys. Rev. Res.* **4**, 043081 (2022).
- [39] A. F. Tzortzakakis, K. G. Makris, and E. N. Economou, Non-Hermitian disorder in two-dimensional optical lattices, *Phys. Rev. B* **101**, 014202 (2020).
- [40] I. Yusipov, T. Laptyeva, S. Denisov, and M. Ivanchenko, Localization in open quantum systems, *Phys. Rev. Lett.* **118**, 070402 (2017).
- [41] N. F. Mott, Conduction in non-crystalline materials, *Philos. Mag. A* **19**, 835 (1969).
- [42] A. Basiri, Y. Bromberg, A. Yamilov, H. Cao, and T. Kottos, Light localization induced by a random imaginary refractive index, *Phys. Rev. A* **90**, 043815 (2014).
- [43] N. Apsley and H. P. Hughes, Temperature-and field-dependence of hopping conduction in disordered systems, *Philos. Mag. A* **30**, 963 (1974).
- [44] N. Apsley and H. P. Hughes, Temperature- and field-dependence of hopping conduction in disordered systems II, *Philos. Mag. A* **31**, 1327 (1975).
- [45] F. Brochard and P. G. de Gennes, Dynamics of confined polymer chains, *J. Chem. Phys.* **67**, 52 (1977).
- [46] Y. C. Zhang, Diffusion in a random potential: Hopping as a dynamical consequence of localization, *Phys. Rev. Lett.* **56**, 2113 (1986).
- [47] J.-P. Bouchaud and A. Georges, Anomalous diffusion in disordered media: Statistical mechanisms, models and physical applications, *Phys. Rep.* **195**, 127 (1990).
- [48] M. Cates and R. Ball, Statistics of a polymer in a random potential, with implications for a nonlinear interfacial growth model, *J. Phys.* **49**, 2009 (1988).
- [49] T. Halpin-Healy and Y.-C. Zhang, Kinetic roughening phenomena, stochastic growth, directed polymers and all that: aspects of multidisciplinary statistical mechanics, *Phys. Rep.* **254**, 215 (1995).
- [50] According to the extreme statistics theory [51,52], the expected largest value $\lambda_{|\mathbf{x}|}^{\max}$ in $n = |\mathbf{x}|^d$ trails taken from the cumulative distribution $F^n(\lambda_{|\mathbf{x}|}^{\max}) = \int_{-\infty}^{\lambda_{|\mathbf{x}|}^{\max}} \rho(\lambda) d\lambda = 1 - P_{|\mathbf{x}|}$ behaves like $F^n(\lambda_{|\mathbf{x}|}^{\max}) \sim 1 - 1/n$, which reproduces $P_{|\mathbf{x}|} \sim 1/n = |\mathbf{x}|^{-d}$.
- [51] A. Hansen, E. L. Hinrichsen, and S. Roux, Non-directed polymers in a random medium, *J. Phys. I* **3**, 1569 (1993).
- [52] E. Gumbel, *Statistics of Extremes*, Dover Books on Mathematics (Dover Publications, New York, 2012).
- [53] See Supplemental Material at <http://link.aps.org/supplemental/10.1103/z9m1-3mwb> for details of calculation.
- [54] Here $\Delta(R)$ is estimated as the typical level spacing within a volume R^3 . We require that at least one state falls within the energy range $\Delta(R)$ at the Fermi energy, which translates to the condition $\Delta(R)R^3\nu \sim 1$, where ν is the density of state at the Fermi energy. This results in the expression $\Delta(R) \sim (1/R^3\nu)$. Substituting this into the optimization equation, one can determine the optimized hopping probability and subsequently derive Mott's relation for conductivity: $\sigma \sim e^{-(T_0/T)^{1/4}}$.
- [55] S.-k. Ma and G. F. Mazenko, Critical dynamics of ferromagnets in $6 - \epsilon$ dimensions: General discussion and detailed calculation, *Phys. Rev. B* **11**, 4077 (1975).
- [56] D. Forster, D. R. Nelson, and M. J. Stephen, Large-distance and long-time properties of a randomly stirred fluid, *Phys. Rev. A* **16**, 732 (1977).
- [57] E. Medina, T. Hwa, M. Kardar, and Y.-C. Zhang, Burgers equation with correlated noise: Renormalization-group analysis and applications to directed polymers and interface growth, *Phys. Rev. A* **39**, 3053 (1989).
- [58] S. Yao and Z. Wang, Edge states and topological invariants of non-Hermitian systems, *Phys. Rev. Lett.* **121**, 086803 (2018).
- [59] S. Yao, F. Song, and Z. Wang, Non-Hermitian Chern Bands, *Phys. Rev. Lett.* **121**, 136802 (2018).

- [60] F. K. Kunst, E. Edvardsson, J. C. Budich, and E. J. Bergholtz, Biorthogonal bulk-boundary correspondence in non-Hermitian systems, *Phys. Rev. Lett.* **121**, 026808 (2018).
- [61] L. Xiao, T. Deng, K. Wang, G. Zhu, Z. Wang, W. Yi, and P. Xue, Non-Hermitian bulk-boundary correspondence in quantum dynamics, *Nat. Phys.* **16**, 761 (2020).
- [62] T. Helbig, T. Hofmann, S. Imhof, M. Abdelghany, T. Kiessling, L. W. Molenkamp, C. H. Lee, A. Szameit, M. Greiter, and R. Thomale, Generalized bulk-boundary correspondence in non-Hermitian topolectrical circuits, *Nat. Phys.* **16**, 747 (2020).
- [63] V. M. Martinez Alvarez, J. E. Barrios Vargas, and L. E. F. Foa Torres, Non-Hermitian robust edge states in one dimension: Anomalous localization and eigenspace condensation at exceptional points, *Phys. Rev. B* **97**, 121401(R) (2018).
- [64] C. H. Lee and R. Thomale, Anatomy of skin modes and topology in non-Hermitian systems, *Phys. Rev. B* **99**, 201103(R) (2019).
- [65] Y. Ashida, Z. Gong, and M. Ueda, Non-Hermitian physics, *Adv. Phys.* **69**, 249 (2020).
- [66] E. J. Bergholtz, J. C. Budich, and F. K. Kunst, Exceptional topology of non-Hermitian systems, *Rev. Mod. Phys.* **93**, 015005 (2021).
- [67] J. T. Gohsrich, A. Banerjee, and F. K. Kunst, The non-Hermitian skin effect: A perspective, *arXiv:2410.23845*.
- [68] Q.-B. Zeng, Y.-B. Yang, and Y. Xu, Topological phases in non-Hermitian Aubry-André-Harper models, *Phys. Rev. B* **101**, 020201(R) (2020).
- [69] B.-B. Wang, Z. Cheng, H.-Y. Zou, Y. Ge, K.-Q. Zhao, Q.-R. Si, S.-Q. Yuan, H.-X. Sun, H. Xue, and B. Zhang, Observation of disorder-induced boundary localization, *Proc. Natl. Acad. Sci. U.S.A.* **122**, e2422154122 (2025).